Analyses of Charge Recombination Process in Organic Electron Luminescence Material with Constrained Density Functional Theory

Analyses of Charge Recombination Process in Organic Electron Luminescence Material with Constrained Density Functional Theory

Koharu AIKAWA

Submitted to
the Graduate School of Pure and Applied Sciences
in Partial Fulfillment of the Requirements
for the Degree of Doctor of Philosophy
in Science
at University of Tsukuba

Doctoral Committee

Professor Kenji Morihashi

Professor Tatsuo Arai

Professor Taka-aki Ishibashi

Professor Kazuya Saito

Contents

1. GENERAL INTRODUCTION 5

2. THEORETICAL BACKGROUND 11

2.1. DENSITY FUNCTIONAL THEORY 11

2.2. CONSTRAINED DENSITY FUNCTIONAL THEORY [13–15] 15

2.2.1. Coupling Matrix Element H_{ab} [15,20,21] 16

2.2.2. Fragmented initial density matrix for CDFT calculations [22] 17

2.2.3. Method for Electron population 17

2.3. MARCUS THEORY 19

3. MOLECULAR ORIENTATION AND CHARGE RECOMBINATION IN POLY(*PARA*-PHENYLENEVINYLENE) 21

3.1. INTRODUCTION 21

3.2. MODELS AND METHODS 24

3.2.1. Models 24

3.2.2. Charge-recombination process calculations 26

3.3. COMPUTAIONAL DETAILS 26

3.4. RESULTS AND DISCUSSION 27

3.4.1. Face-to-face orientation and the center-to-center distance 27

3.4.2. Effect of the roll angle 30

3.4.3. Effect of the intermolecular distance in edge-to-face conformation . 34

3.5. CONCLUSIONS 38

4. EFFECT OF CONJUGATION LENGTH OR SIDECHAINS FOR CHARGE RECOMBINATION IN POLY(PARA-PHENYLENEVINYLENE) 41

4.1. INTRODUCTION 41

4.2. MODELS AND METHODS 42

4.2.1. Models 42

4.2.2. Computational methods 44

4.2.3. Estimating Marcus parameters 45

4.3. COMPUTATIONAL DETAILS 45

4.4. RESULTS AND DISCUSSION 45

4.5. CONCLUSIONS 50

5. GENERAL CONCLUSIONS 52

6. REFERENCES 54

PUBLICATION LIST 60

MAIN PAPERS 60

OTHERS 60

1. General Introduction

Organic semiconductors, which are used in organic light-emitting diodes (OLEDs), organic field-effect transistors (OFETs), and organic solar cells, attracted considerable interest because of their charge-transport properties. The performance of organic semiconductors has been enhanced to match that of inorganic semiconductor such as silicon as reported in recent studies [1–5]. In most of these studies, intensive effort has been devoted to enhancing the charge mobility, which is an important factor when evaluating the performance of organic semiconductors [6–9].

OLEDs have gained prominence as a new technology for displays and illuminations. OLEDs exploit the advantages of flexible, lightweight, workable, and low cost materials. These features are very attractive for application in daily life. However, the performance of OLEDs is still unsatisfactory for widespread application because the quantum efficiency of the electroluminescence is low in practice. Therefore, extensive research has been devoted studying the phenomena of the emission phenomena of OLEDs to understand the fundamental mechanisms, to garner understanding for developing materials with higher efficiency [4,6,10–24], and to improve the emission efficiency of OLEDs. In this thesis, we investigate the charge-recombination process, specifically in OLED emission.

The charge-recombination process in OLEDs is the final process prior to emission. This involves the collapse of the positive and negative charges after the moving positive or negative charge is injected from the electrode. This process puts the system in the

excited state, and the excited-state molecule emits photons in the OLEDs. This process strongly influences the emission efficiency of OLEDs. However, it is difficult to observe this process experimentally. Thus, we tackled this process via the computational approach to enable investigation of the mechanism.

Among several computational methods, the *ab initio* approach provides a reliable way to approximately solve the Schrödinger equation for electrons in atoms and molecules. Because the *ab initio* method describes the electronic structure with molecular orbitals, we can analyze systems at the quantum mechanical level. In particular, density functional theory (DFT) is the most popular method used in computational quantum chemistry. DFT can describe the electron correlation effect with low computational cost as compared to post-Hartree-Fock theories, *e.g.* configuration interaction, Møller-Plesset perturbation theory, coupled cluster theory, etc. However, DFT tends to delocalize electrons in the systems due to the self-interaction error. Hence, conventional DFT cannot suitably describe the charge-separated state, where one side is positively charged and the other side is negatively charged.

This thesis required the computational scheme using constrained density functional theory (CDFT) because the CT-state dimer is a charge-separated system. CDFT can suitably treat charge-separated systems that conventional DFT fails to describe. CDFT was developed by Van Voorhis, and coauthors [25–30], and has attracted the attention of many researchers [24,29,31–36]. However, CDFT does not have a good convergence due to several technical difficulties. Therefore we improved the generation scheme of the initial density matrix [37]. Treating a dimer system, the initial density matrix of the

dimer is generated by combination of the monomer density matrices. We found that this technique enables reduction of the number of required CDFT-SCF cycles and shortens the time required for convergence. CDFT describes the charge-separated state, which is difficult to compute using conventional DFT; thus, the former permits detailed evaluation of the charge-recombination process. Moreover, CDFT can be widely applied to inter-molecular electron separated systems. This technique is also applied to dividing methods such as the fragment Kohn-Sham (f-K-S) method [38] for large biological systems, proteins and DNA, and can circumvent several shortcomings of the f-K-S method.

We used an approach termed the "four-point method" based on Marcus theory because the charge-recombination reaction is a type of electron-transfer reactions. The four-point method is a simple way to estimate the parameters of the Marcus-Hush equation, *i.e.* the reorganization energy λ, the driving force $-\Delta G^0$, the activation energy $\Delta G^{\ddagger}$, and the coupling matrix element H_{ab} [39]. The Marcus-Hush equation based on Marcus theory is defined to estimate the electron-transfer rate constant. The four points combine the electron states and the reaction coordinates (*i.e.* the structure) of the initial and final states. In the four-point method, the parameters of the Marcus-Hush equation, except for the coupling matrix element are defined by the difference between the energies of the four points. The coupling matrix element is obtained by the approach based on CDFT, which was developed by Wu and Voorhis [28].

For some of the OLEDs materials, we focused on poly-*para*phenylenevinylene (PPV; Scheme 1-1), which is a polymer of phenylenevinylene. PPV is a currently

well-researched OFET material [4,10,15,40–54]; for example, the high quantum efficiency of the derivatives of PPV as an OLED material has been reported by Cao et al. [55]. Herein, focus was placed on investigating the intermolecular orientation, the conjugation length, and the side-chain effects at the oligomer level as a model "chromophore". When PPV is used as an OLED material, the emitting layer of PPV becomes amorphous. This layer contains the "chromophores", which are the sequential conjugated units. In the amorphous form of PPV, the chromophores adopt many orientations. PPV is an amenable system for evaluation of the orientation because the PPV has a planar structure. Moreover, the chromophores are easily defined as the model system, because if the structure adopts a planar configuration, it is conjugated.

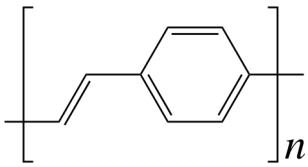

Scheme 1-1. Chemical structure of PPV, where *n* is the polymerization number.

For the CDFT calculation, the dimer model system was developed by combining the donor and the acceptor of oligo-*para*phenylenevinylene (OPV). We employed OPV, which is a congener of PPV with reduced number of units, for the model systems because PPV is too large for computational analysis. We consider two states of the charge-recombination process: the initial state (before charge-recombination) and the final state (after the charge-recombination). The initial state is the charge-separated state, which is described as the system combining the radical anion as the electron donor

molecule and the radical cation as the electron acceptor molecule. The final state is the exciton state, which is a dimer state in which the ground and excited states of the OPV monomer are combined.

In this study, we found that the orientation in the collapsing injected-charge region, the length of the chromophores, and the substitution of bulky electron-donating side-chains are important factors influencing the emission efficiency of PPV. These findings should aid the development of high-performance OLED materials. OLED displays are not popular at present; however, the present studies about OLEDs sould lead to the development of OLEDs with lower prices, longer life, and eco-friendliness. Further, we suggest that the CDFT-approach used in this thesis is a powerful tools for computation of the electron-transfer systems that are difficult for the conventional DFT and the post Hartree-Fock theories to describe.

It is found that the recombination reaction of PPV lies in the Marcus inverted region, which is considered to be the general trend for the charge-recombination of PPV. This means that the rate constant of the charge-recombination reaction decreases with an increase of the driving force $-\Delta G^0$. In the "normal region", on the other hand, the electron-transfer rate constant increases with increasing driving force.

The structure of this thesis is as follows: in Chapter 2, we explain the theoretical background of this work including how to compute the electron-transfer rate. In particular, DFT and Marcus theory are explained. In Chapter 3, we discuss the charge recombination rate constant and the intermolecular orientations in three OPV units referred to as OPV3. We investigate the charge recombination rate constants for various

intermolecular orientations of the dimer system, where either the donor or the acceptor molecule rotates along the molecular axis. It is suggested that the rotations of the acceptor molecule promote the charge-recombination reaction and that rotation of the donor molecule hinders the charge-recombination reaction. In Chapter 4, the conjugation length and the side-chain effect for the charge recombination rate constant of the OPV*n* are discussed. The effect of the conjugation length is evaluates based on the *n*-dependency of OPV unit (*n*=2~4) and the effect of terminal groups with/without extended conjugation. We also investigate the side-chain effect by focusing on OPV3 derivatives modified with ethoxy, cyano and fluoro groups. The data suggests that the charge-recombination reaction occurs and that the large size electron donating side-chains facilitate charge-recombination with increasing conjugation length. Finally, the general conclusions are presented in Chapter 5.

2. Theoretical background

2.1. Density Functional Theory

Molecular orbital theory as Hartree-Fock (HF) method is used for the electronic structure calculation of molecules. However, since Kohn-Sham method is developed in 1965, density functional theory (DFT) started has been used for many-body problems in atoms and molecules. Recently, DFT is widely applied to various fields, *i.e.*, solid states, biological systems.

The original idea of DFT was proposed by Thomas and Fermi, who suggested that the fundamental variation of a system is the electron density $\rho(\mathbf{r})$ instead of wave function, and after a few years their theory was expanded by Dirac. Now their theory is called as Thomas-Fermi-Dirac model [56–58], or orbital free model. The functional of energy for atomic systems is written as

$$E_{\mathrm{TFD}}[\rho(\mathbf{r})] = C_{\mathrm{F}} \int \rho^{5/3}(\mathbf{r}) \mathrm{d}\mathbf{r} - Z \int \frac{\rho(\mathbf{r})}{r} \mathrm{d}\mathbf{r} + \frac{1}{2} \iint \frac{\rho(\mathbf{r}_1)\rho(\mathbf{r}_2)}{|\mathbf{r}_1 - \mathbf{r}_2|} \mathrm{d}\mathbf{r}_1 \mathrm{d}\mathbf{r}_2 \quad \ldots (2.1)$$

where the first term in the right side is kinetic energy $T[\rho]$, the second term is nuclear-electron attraction energy integral $V_{ne}[\rho]$, and the third term is Coulomb integral $J[\rho]$.

Furthermore, the integral of the electron density over all space equals the total electron number.

$$\int \mathrm{d}\mathbf{r} \rho(\mathbf{r}) = N. \quad \ldots (2.2)$$

The minimization of $E[\rho]$ using Lagrange multiplier method with the above constraint can get the atomic energy.

$$\Omega_{\mathrm{TFD}}[\rho] = E_{\mathrm{TFD}}[\rho] - \mu\left\{\int \mathrm{d}\mathbf{r}\rho(\mathbf{r}) - N\right\} \quad \ldots(2.3)$$

Two Hohenberg-Kohn (H-K) theorems [59] were established from this. The first H-K theorem is that the external potential $v(\mathbf{r})$ is uniquely determined by the ground state density $\rho(\mathbf{r})$. From this theorem, E_v, which E determined for v, is written as

$$\begin{aligned} E_v[\rho] &= T[\rho] + V_{ee}[\rho] + V_{ne}[\rho] \\ &= F_{\mathrm{HK}}[\rho] + \int \rho(\mathbf{r})v(\mathbf{r})\mathrm{d}\mathbf{r}, \end{aligned} \quad \ldots(2.4)$$

$$F_{\mathrm{HK}}[\rho] = T[\rho] + V_{ee}[\rho]. \quad \ldots(2.5)$$

The second H-K theorem is that the two energies must obey the variational principle. *i.e.* if the trial density function $\tilde{\rho}(\mathbf{r})$ is $\tilde{\rho}(\mathbf{r}) \geq 0$ and $\int \tilde{\rho}(\mathbf{r})\mathrm{d}\mathbf{r} = N$, $E[\rho]$ must be grater than or equal to the true ground state energy E_0.

Moreover Kohn-Sham method [60] was made for applying those theories for the practical problems. Kohn and Sham rewrote the kinetic energy T_s for electrons without the interaction as

$$\begin{aligned} T_s[\rho] &= \sum_i^N \left\langle \psi_i \right| -\frac{1}{2}\nabla^2 \left| \psi_i \right\rangle, \\ \rho(\mathbf{r}) &= \sum_i^N \sum_s \left|\psi_i(\mathbf{r}, s)\right|^2. \end{aligned} \quad \ldots(2.6)$$

It can rewrite F as

$$F[\rho] = T_s[\rho] + J[\rho] + E_{xc}[\rho], \quad \ldots(2.7)$$

where exchange-correlation enegy, E_{xc}, is defined as

$$E_{xc}[\rho] = T[\rho] - T_s[\rho] + V_{ee}[\rho] - J[\rho]. \quad \ldots(2.8)$$

Then, Lagrange multiplier is defined as

$$\mu = v_{eff}(\mathbf{r}) + \frac{\delta T_s[\rho]}{\delta\rho(\mathbf{r})}, \quad \ldots(2.9)$$

where KS effective potential, $v_{eff}(\mathbf{r})$, is defined as

$$\begin{aligned} v_{eff}(\mathbf{r}) &= v(\mathbf{r}) + \frac{\delta J[\rho]}{\delta\rho(\mathbf{r})} + \frac{\delta E_{xc}[\rho]}{\delta\rho(\mathbf{r})} \\ &= v(\mathbf{r}) + \int \frac{\rho(\mathbf{r}')}{|\mathbf{r}-\mathbf{r}'|} \mathrm{d}\mathbf{r}' + v_{xc}(\mathbf{r}), \end{aligned} \quad \ldots(2.10)$$

$$v_{xc}(\mathbf{r}) = \frac{\delta E_{xc}[\rho]}{\delta\rho(\mathbf{r})}. \quad \ldots(2.11)$$

In Kohn-Sham method, the equation is solved by the constraint with the effective potential:

$$\left[-\frac{1}{2}\nabla^2 + v_{eff}(\mathbf{r})\right]\psi_i = \varepsilon_i\psi_i \quad \ldots(2.12)$$

The most important feature of DFT is that DFT can include the electron correlation effect relatively easer than the post Hartree-Fock (H-F) theories. The post H-F theories such as configuration interaction (CI) and Møller-Plesset perturbation theory [61] need sophisticate calculations to include the electron correlation effect. Those methods are very high-computational cost, and further CI method is not free from the size-inconsistency problem. On the other hand, DFT can consider the electron correlation effect without sophisticate calculation, where the electron correlation effect is implicitly included through the exchange-correlation functional form.

2.1.1. Local Density Approximation

Since the exact exchange-correlation functional E_{xc} expression is not found yet, we apply the approximation for E_{xc}. The simplest approximation is "local density approximation" (LDA):

$$E_{xc}^{\mathrm{LDA}}[\rho] = \int \rho(\mathbf{r})\varepsilon_{xc}\, d\mathbf{r}\,, \quad (2.13)$$

where ε_{xc} is the exchange-correlation energy in the local density ρ of a uniform electron gas. [62,63]

2.1.2. General Gradient Approximation

However, because the local density does not change around all over the system in the LDA approximation, the exchange-correlation energy tends to be overestimated. Therefore several types of exchange-correlation functional were developed, e.g. generalized gradient approximations (GGAs), meta-GGAs, and hybrid functionals.

2.1.3. B3LYP functional

To use density functional theory for the practical problems such as electrons in atoms, molecules and solids, we should choose the good exchange-correlation functional for the system that we want to know. B3LYP [64], which is I used in this thesis, is a hybrid functional and the most popular functional for treating molecular systems. Hybrid functional is developed from a combination with the exchange-correlation functionals and the Hartree-Fock *exact* exchange functional. The exact exchange functional improves the effect around the interacting regions. The exchange-correlation functional set of B3LYP is given by:

$$E_{XC} = E_{XC}^{LSDA} + a_0(E_X^{\text{exact}} - E_X^{\text{LSDA}}) + a_X \Delta E_X^{\text{B88}} + a_C \Delta E_C^{\text{PW91}}, \qquad (2.14)$$

where a_0, a_X, and a_C are semi-empirical coefficients (each values are optimized to 0.20, 0.72, and 0.81), E_X^{exact} is the *exact* exchange energy, ΔE_X^{B88} is Becke's 1988 gradient correction (for LSDA) for exchange, and ΔE_C^{PW91} is the 1991 gradient correction for correlation by Perdew and Wang. [64] This functional shows very good accuracy for

various systems in computational chemistry.

2.2. Constrained Density Functional Theory

In DFT, the delocalized electronic structure is erroneously estimated to be a more stable state than the charge-localized structure owing to the self-interaction error. [65] For this reason, several methods have been developed to correct this error: the self-interaction correction by Perdew and Zunger, [66] the DFT+U method using the Hubbard U model, [67] the long-range correction scheme, [68] and the constrained DFT (CDFT). Especially, CDFT is a method which imposes constraints on the charge or spin density of arbitrary molecular fragments [25,26,29].

In CDFT, the difference in the charge or spin density between arbitrary fragments is constrained. A general constraint on the density is described as

$$\sum_{\sigma} \int w_c^{\sigma}(\mathbf{r}) \rho(\mathbf{r}) \mathrm{d}\mathbf{r} = N_c , \qquad \ldots(2.15)$$

where $w_c(\mathbf{r})$ is the weight function that defines the constrained property, ρ is the charge density, σ represents the α or β spin, and N_c is the net difference in charge between the donor and the acceptor, i.e., $N_c = (N_\mathrm{D} - N_\mathrm{A})/2$. The weight function is $w_c^{\alpha} = -w_c^{\beta}$ for the spin constraint. The following energy functional, which is added to this constraint term via a Lagrange multiplier V_c, is minimized during the SCF optimization.

$$W[\rho, V_c] = E[\rho] + V_c \left(\sum_{\sigma} \int w_c^{\alpha}(\mathbf{r}) \rho(\mathbf{r}) \mathrm{d}\mathbf{r} - N_c \right). \qquad \ldots(2.16)$$

Here, we demonstrate a typical example of the constraint term in CDFT when the region C is constrained as shown in Figure 2-1. First, if the charge density is constrained, then

$$\left(\int_{\mathrm{C}}\rho^{\alpha}(\mathbf{r})\mathrm{d}\mathbf{r}+\int_{\mathrm{C}}\rho^{\beta}(\mathbf{r})\mathrm{d}\mathbf{r}\right)-\left(\int_{\mathrm{NC}}\rho^{\alpha}(\mathbf{r})\mathrm{d}\mathbf{r}+\int_{\mathrm{NC}}\rho^{\beta}(\mathbf{r})\mathrm{d}\mathbf{r}\right)$$
$$=\int_{\mathrm{C}}\rho(\mathbf{r})\mathrm{d}\mathbf{r}-\int_{\mathrm{NC}}\rho(\mathbf{r})\mathrm{d}\mathbf{r}=N_{\mathrm{C}}-N_{\mathrm{NC}}=N_c. \quad \ldots(2.17)$$

On the other hand, if the spin density is constrained, then

$$\left(\int_{\mathrm{C}}\rho^{\alpha}(\mathbf{r})\mathrm{d}\mathbf{r}-\int_{\mathrm{C}}\rho^{\beta}(\mathbf{r})\mathrm{d}\mathbf{r}\right)-\left(\int_{\mathrm{NC}}\rho^{\alpha}(\mathbf{r})\mathrm{d}\mathbf{r}-\int_{\mathrm{NC}}\rho^{\beta}(\mathbf{r})\mathrm{d}\mathbf{r}\right)$$
$$=\int_{\mathrm{C}}\rho^{s}(\mathbf{r})\mathrm{d}\mathbf{r}-\int_{\mathrm{NC}}\rho^{s}(\mathbf{r})\mathrm{d}\mathbf{r}=N_c, \quad \ldots(2.18)$$

where ρ^s is the spin density.

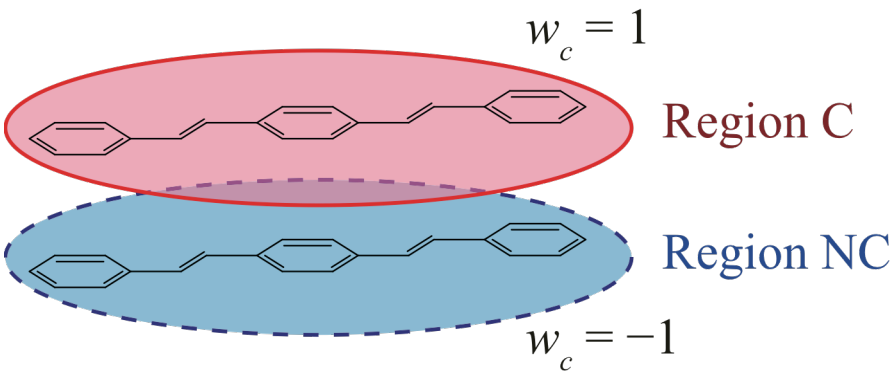

Figure 2-1. Region C is constrained region, and Region NC is non-constrained region.

2.2.1. Coupling Matrix Element H_{ab}

Furthermore, Wu and Van Voorhis have developed a CDFT method to calculate the electronic coupling matrix element H_{ab} [28,29,34]. The following matrix H is obtained by using $V_c w_c$ solved in the CDFT calculation:

$$\mathbf{H}=\begin{pmatrix} H_{\mathrm{DD}} & H_{\mathrm{DA}} \\ H_{\mathrm{AD}} & H_{\mathrm{AA}} \end{pmatrix}, \quad \ldots(2.19)$$

where the matrix elements are

$$H_{\mathrm{DD}}=\langle\Phi_{\mathrm{D}}|H|\Phi_{\mathrm{D}}\rangle=E[\rho_{\mathrm{D}}]=E_{\mathrm{D}} \quad \ldots(2.20)$$

$$H_{\mathrm{AA}} = E_{\mathrm{A}} \qquad \ldots(2.21)$$

$$\begin{aligned} H_{\mathrm{DA}} &= \left\langle \Phi_{\mathrm{D}} \middle| H + V_c^A w_c - V_c^A w_c \middle| \Phi_{\mathrm{A}} \right\rangle \\ &= F_{\mathrm{A}} \left\langle \Phi_{\mathrm{D}} \middle| \Phi_{\mathrm{A}} \right\rangle - V_c^{\mathrm{A}} \left\langle \Phi_{\mathrm{D}} \middle| w_c \middle| \Phi_{\mathrm{A}} \right\rangle \end{aligned} \qquad \ldots(2.22)$$

$$H_{\mathrm{AD}} = F_{\mathrm{D}} \left\langle \Phi_{\mathrm{A}} \middle| \Phi_{\mathrm{D}} \right\rangle - V_c^{\mathrm{D}} \left\langle \Phi_{\mathrm{A}} \middle| w_c \middle| \Phi_{\mathrm{D}} \right\rangle \qquad \ldots(2.23)$$

and

$$F = \left\langle \Psi_{\mathrm{D}} \middle| H + V_c^A w_c \middle| \Psi_{\mathrm{A}} \right\rangle = E[\rho_c] + V_c \int w_c(\mathbf{r}) \rho(\mathbf{r}) \mathrm{d}\mathbf{r} = E + V_c N_c. \qquad \ldots(2.24)$$

By orthogonalization between Φ_{D} and Φ_{A}, we can obtain the coupling matrix element H_{ab} as the off-diagonal element.

2.2.2. Fragmented initial density matrix for CDFT calculations

To improve the convergence in the CDFT calculations, we applied the fragmented initial density matrix comprising the monomer charge densities. For instance, in Figure 2-1 the charge density matrices $\mathbf{D}_1$ of Region C and $\mathbf{D}_2$ of Region NC are put on the diagonal blocks of the initial density matrix of the dimer as follows:

$$\mathbf{D} = \begin{pmatrix} \mathbf{D}_1 & 0 \\ 0 & \mathbf{D}_2 \end{pmatrix}. \qquad \ldots(2.25)$$

Using this initial density matrix can decrease the number of required CDFT-SCF cycles and speed up the convergence. We confirmed that the computational results agreed with those obtained without using the fragmented initial density matrix in several test calculations [37].

2.2.3. Method for Electron population

In molecular systems, the well known methods to partition the total electron density

into each atom, *i.e.*, atomic population schemes, were developed by Mulliken [69], Löwdin [70], and Becke [71]. In this thesis, we used Becke's multicenter integration scheme for the weight function in the CDFT calculations because we found after several test calculations that Becke scheme is best for CDFT among those schemes.

Becke's multicenter integration scheme uses *fuzzy cell* to softly divide the system. First, fuzzy cell requires the two-center coordinate system and defines μ as

$$\mu_{ij} = \frac{r_i - r_j}{R_{ij}}, \qquad \ldots(2.26)$$

where, r_i and r_j denote the distances of electron to nuclei i and j, and R_{ij} is the inter-nuclar separation. Next, an odd function f and a two-term polynomial p are made for a cell function P.

$$\begin{aligned} f_3(\mu) &= p\{p[p(\mu)]\}, \\ p(\mu) &= \tfrac{3}{2}\mu - \tfrac{1}{2}\mu^3, \end{aligned} \qquad \ldots(2.27)$$

$$P_i(\mathbf{r}) = \prod_{j \neq i} \tfrac{1}{2}\left[1 - f_3(\mu_{ij})\right]. \qquad \ldots(2.28)$$

The electron density is defined by a weight function w_n using the cell function.

$$w_n(\mathbf{r}) = \frac{P_n(\mathbf{r})}{\sum_m P_m(\mathbf{r})} \qquad \ldots(2.29)$$

$$N = 2\sum_n^{N/2} \int w_n(\mathbf{r})\rho(\mathbf{r})\mathrm{d}\mathbf{r} \qquad \ldots(2.30)$$

In CDFT, the weight function is defined from this electron population scheme.

$$\left(w_c\right)_{\lambda\nu} = \sum_{n \in C} \phi_\lambda(\mathbf{r}) w_n(\mathbf{r}) \phi_\nu(\mathbf{r})\mathrm{d}\mathbf{r} \qquad \ldots(2.31)$$

2.3. Marcus theory

In this thesis, we used the theory for the rates of non-adiabatic electron transfer reaction proposed by R. A. Marcus [72]. If the electron-transfer reaction behaves on Franck-Condon principle, *i.e.* the inner and outer reorganization occur after the electron transfer, the energy diagram is illustrated as Figure 2-2.

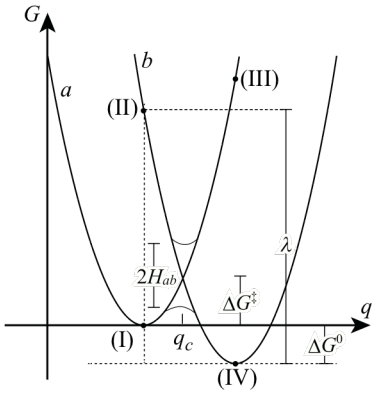

Figure 2-2. Schematic free-energy curves obtained by Marcus theory for the electron-transfer (ET) process. Parabolas *a* and *b* are the initial and final electronic states, respectively. Points (I) and (III) represent the geometry of initial state in the ET reaction and points (III) and (IV) represent the geometry of final states.

By using CDFT, we estimated the driving force, $-\Delta G^0$, the reorganization energy, λ using the four-point method [39]:

$$\Delta G^0 = E(Q_f//\Phi_f) - E(Q_i//\Phi_i), \quad \ldots(2.32)$$

$$\lambda = E(Q_i//\Phi_f) - E(Q_f//\Phi_f), \quad \ldots(2.33)$$

where Q_f and Q_i are the geometries of the final and initial states, respectively, and Φ_f and Φ_i are the electronic states of the final and initial states, respectively. The corresponding combination of the molecular structure and the electronic structure for Figure 2-2 are shown in Table 2-1.

Table 2-1. Molecular and electronic structures at the four points in Figure 2-2.

System	Molecular structure	Electronic structure
(I)	Q_i	Φ_i
(II)	Q_i	Φ_f
(III)	Q_f	Φ_i
(IV)	Q_f	Φ_f

In this situation, the electron-transfer rate constant is described by Marcus-Hush equation as

$$k_{\mathrm{ET}} = \frac{2\pi}{\hbar}\frac{1}{\sqrt{4\pi\lambda k_{\mathrm{B}}T}}H_{ab}^{2}\exp\left(-\frac{(\Delta G^{0}+\lambda)^{2}}{4\lambda k_{\mathrm{B}}T}\right), \qquad \ldots(2.34)$$

where k_{B} and $\hbar$ are the Boltzmann and Dirac constants, respectively, k_{ET} is the electron transfer rate constant, T is the absolute temperature, and H_{ab} is the coupling matrix element. Then, the activation energy $\Delta G^{\ddagger}$ is defined as

$$\Delta G^{\ddagger} = \frac{(\Delta G^{0}+\lambda)^{2}}{4\lambda}. \qquad \ldots(2.35)$$

From this equation, it is found that $\Delta G^{\ddagger} = 0$ if $-\Delta G^{0} = \lambda$, $\Delta G^{\ddagger} > 0$ if $-\Delta G^{0} < \lambda$ or $-\Delta G^{0} > \lambda$, and that $\Delta G^{\ddagger}$ is greater with increasing the absolute value of $(\Delta G^{0} + \lambda)$. When $-\Delta G^{0} > \lambda$, it is called "inverted region". The inverted region is first reported in the study of charge recombination reaction by Miller [73] and studied for the various systems.

3. Molecular Orientation and Charge Recombination in Poly(*para*-phenylenevinylene)

3.1. Introduction

The emissive electroluminescence layer of OLED is a film of an organic semiconductor. OLEDs often use a thin polymer film fabricated by vacuum evaporation/sublimation or solution-casting or printing technologies. In the case of solution-casting technology, the performance of the OLEDs is strongly affected by the type of solution. For example, a poly-*para*phenylenevinylene (PPV)-based polymer film with chlorobenzene solvent exhibits larger field-effect hole mobility than one with toluene. This difference in the hole mobility is attributed to the difference in the molecular alignment in the film [41,74].

Generally, π-conjugated molecules such as PPV often aggregate in a π-stacked form [75,76]. These π-stacked structures have a large transfer integral; this parameter represents the probability of adiabatic electron transfer (ET) in the conjugated material [3,6,77,78]. On the other hand, the mobilities in the crystalline derivative of tetrathiafulvalene increase in the order of partial stacking, lamella (stacking), and the herringbone structure. Similarly, the herringbone structures of rubrene and tetracene exhibit very high mobilities of 24.5 and 5 $cm^2\ V^{-1}\ s^{-1}$, respectively. According to previous studies, these high mobilities in the herringbone structure are due to the small grain-boundary effect [1] and the small electro static repulsion in the herringbone structure [2] than that in the π-stacked structure. This indicates that the transfer integral

alone is insufficient to discuss the ET reaction. We focus on not only the transfer integral but also the other parameters in Marcus theory: the driving force $-\Delta G^0$ and reorganization energy λ. As explained in Section 3.2.2, because these parameters are inside the exponential in the equation for the ET rate constant (equation (1)).

PPV is used in OFETs such as OLEDs and in organic solar cells using the opposite reaction to that in OLEDs [4]. PPV has thus attracted considerable attention as an OLED material [43]. The working principle of the luminescence process of PPV as an OLED material is based on charge injection as shown in Figure 3-1; first, electrons and holes are injected from the electrodes to the PPV layer, and the collision between holes and electrons with charge recombination induces an ET reaction. Then the holes and electrons form excited acceptor molecules, and the PPV emits light when it returns to the ground state.

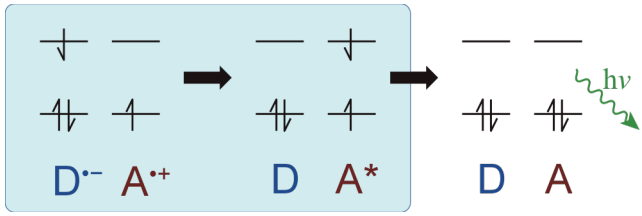

Figure 3-1. Luminescence process based on charge injection. The blue shaded area shows the charge recombination process focused on in this study. D and A represent the donor and acceptor molecules, respectively. In this study, we concentrate the triplet-triplet charge recombination process.

The maximum ratio of the quantum efficiencies for electroluminescene and photoluminescenece (QE(EL)/QE(PL)) is theoretically 25% because of the generation ratio of the singlet to the triplet. However, Cao *et al.* [55] have measured the efficiency of PPV-based OLEDs to be as high as ~50% in experiments. To clarify the origin of

such a high efficiency, Shuai *et al.* [79] investigated the behavior of excitons within the π-electron approximation. According to their results, a high efficiency is achieved in the coherent electronic state, *i.e.*, strong coupling. However, heir study did not consider the structural dependence, that is, hey computed only cofacial arrangement in which PPV molecules were separated by 4.0 Å in their model of the bulk structure of PPV.

In this thesis, we provide new perspectives that are different from those in previous studies concerning the use of PPV as an organic semiconductor in the following two points. First, previous studies discussed hole and/or electron transfer but not the charge recombination process. Second, these studies included the orientations applied for the model system of PPV treat only shifted on face-to-face orientation or yawing by Euler angle (the rotation of the molecule around the vertical axis for a plane) [2,79–82], even though the crystal structure of PPV has a rolled or pitched structure and a similar structure can appear in a thin film of PPV. The crystal structure of PPV has herringbone packing [83]. The setting angle in the structure has been estimated to be between 56 and 68˚. If PPV forms a thin film, its morphology will be amorphous. According to previous experimental study, the structure is cylindrical with a local stack structure, and its horizontal cross section has the edge-to-face form [84]. In this study, we focus on the charge-recombination process, which is the final state before the luminescence process, and the molecular alignments in the case of cofacial π-stacks and roll displacements.

We calculate the charge recombination process and the Marcus parameters for the charge recombination process of PPV using constrained density functional theory (CDFT; details in Section 2.2) [25,26,28,29,85]. Although the charge recombination

rate constant of the cofacial orientation in our study is very small (on the order of 10^{-18}), several rotations result in a large recombination rate constant of up to ~10^{8}. Further, we show that the angle of rotation is considerably different for the donor and acceptor molecules.

3.2. Models and Methods

3.2.1. Models

Because PPV polymers are too large for CDFT calculations, we used oligo-paraphenylene vinylene, which contains three units (OPV3), as a model system for PPV. The dimer system consists of two molecules that are donor and acceptor molecules. The initial state of OPV3 dimer is the complex of the radical anion ($D^{\bullet-}$) and radical cation ($A^{\bullet-}$) OPV3 monomer (*i.e.,* polaron pair), which we represent as $\{D^{\bullet-}\ldots A^{\bullet+}\}$. The final state of the OPV3 dimer is the complex of the ground state (^{1}D) and T1 excited state ($^{3}A^{*}$) of OPV3 monomer (i.e., exciton pair), we represent as $\{^{1}D\ldots{}^{3}A^{*}\}$. The monomer structures, $D^{\bullet-}$, $A^{\bullet+}$, ^{1}D, and $^{3}A^{*}$, for generating dimer pairs are optimized, respectively, and arranged as the dimer systems.

The molecular center-to-center distance in the face-to-face dimer is set to be 4.0 Å, similar to the reported in previous studies [79–81]. Upon rotational orientation, the donor or acceptor of the dimer is rotated around the principal axis of inertia (the *x*-axis in Figure 3-2). We refer to this as roll rotation by the Euler angle.

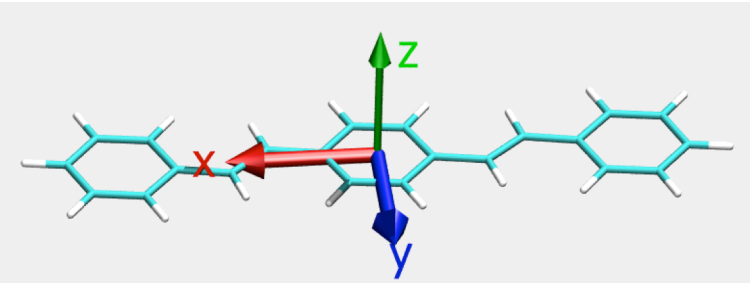

Figure 3-2. Principal axis of inertia of OPV3.

In tilted orientations, the default site-site distance was set to be 2.9 å for the closest hydrogen-hydrogen distance between the tilted and planar sites (Figure 3-3).

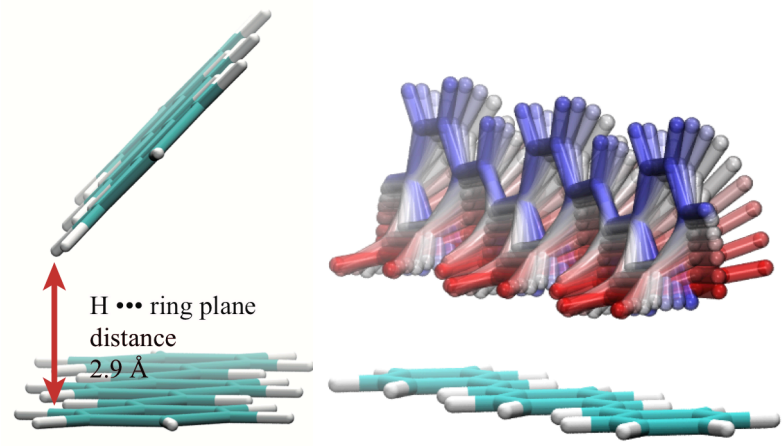

Figure 3-3. Closest-contact distance when the upper molecule is tilted (left) and rotated from 10° to 90° (right).

In the investing of the possible form of the dimer in the charge-recombination process of OPV3, the charge transfer properties of the crystal form will provide information on the likely OPV3-dimer system. However, we have no data for the OPV3 crystal. As an alternative, to find the likely OPV3-dimer form, we investigate the methyl-substituted OPV3 (OPV3-methyl, Scheme 3-2) system, because the single-crystal structure has been determined by X-ray analysis. Thus, the geometric alignment of the OPV3-methyl

dimer that minimizes the root-mean-square deviation for the crystal structure was calculated using '*Pair Fitting*' in PyMOL.

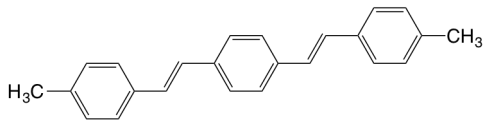

Scheme 3-2. OPV3-methyl

3.2.2. Charge-recombination process calculations

We focus on the charge-recombination factor k_{CR} and its parameters in the Marcus-Hush equation, i.e., the reorganization energy λ, the driving force $-\Delta G^0$, and the transfer integral H_{ab}. Using Marcus theory, we predict k_{CR} and the parameters of the four states, which can be represented as combinations of the electronic and molecular structures of the initial and final states shown in Figure 2-2 and Table 3-2.

Table 3-2. Molecular and electronic structures at the four points in Figure 2-2.

System	Molecular structure	Electronic structure
(I)	$\{D^{\bullet-}\text{-}A^{\bullet+}\}$	$\{D^{\bullet-}\text{-}A^{\bullet+}\}$
(II)	$\{D^{\bullet-}\text{-}A^{\bullet+}\}$	$\{^1D\text{-}^3A^*\}$
(III)	$\{^1D\text{-}^3A^*\}$	$\{D^{\bullet-}\text{-}A^{\bullet+}\}$
(IV)	$\{^1D\text{-}^3A^*\}$	$\{^1D\text{-}^3A^*\}$

3.3. Computational Details

Geometry optimization of the monomers was performed at the B3LYP/6-31G(d) level with the Gaussian09 package. Dimer calculation by CDFT was performed using a program developed in our laboratory at the same level of theory. In all CDFT

calculations, we used the Becke weight population scheme to define the weight functions. The electronic coupling matrix element H_{ab} was calculated using the Kohn-Sham orbitals and the parameters V_c in the dimer calculations using our program. In addition, we used the fragment initial density matrix to improve the convergence performance.

3.4. Results and Discussion

3.4.1. Face-to-face orientation and the center-to-center distance

The calculation for OPV3 and OPV3-methyl were performed in the face-to-face orientation (at a fixed center-to-center distance of 4.0 Å). Although the face-to-face orientation has been used in many previous studies, the charge-recombination rate of the orientation obtained in the present work using the CDFT calculation is very small (10^{-18} s^{-1} order). These parameters and the charge recombination factor of OPV3 and OPV3-methyl are shown in Table 3-3, and the relative energies of the four states (in Table 3-2 and Figure 2-2) are shown in Table 3-4.

Table 3-3. Calculated charge recombination parameters and the decadic logarithm of the charge recombination rate in the face-to-face orientation of the OPV3 and OPV3-methyl systems

System	$-\Delta G^0$	λ	$\Delta G^{\ddagger}$	$\lvert H_{ab}\rvert$	$\log_{10}(k_{CR}[s^{-1}])$
Face-to-face OPV3	162.7	25.15	188.0	19.40	−17.80
Face-to-face OPV3-methyl	155.7	25.82	163.3	20.44	−13.45

All energies are in kJ mol^{-1}

Table 3-4. Calculated energies of four states in Figure 2-2 in the face-to-face orientation of the OPV3 and OPV3-methyl systems

System	(I)	(II)	(III)	(IV)
face-to-face OPV3	0.000	−137.5	25.43	−162.7
face-to-face OPV3-methyl	0.000	−129.9	26.39	−155.7

All energies are in kJ mol^{-1}

When the center-to-center distance of OPV3 is increased, the recombination rate decreases as shown in Figure 3-4. Figure 3-5 shows the energy variations of the four states with the center-to-center distance of the OPV3 dimer. The energy gaps between the initial states (I) and (III) and between the final states (II) and (IV) become larger as the distance increases. This indicates that PPV in the cofacial orientation has a large driving force in the case of a large intermolecular distance. Because the energies of the four states increase with decreasing center-to-center distance below 4.0 because of the van der Waals repulsion, as shown in Figure 3-5, the center-to-center distance at which CR is induced is estimated to be over 4.0 Å. In the face-to-face orientation, the recombination rate is less than 1 s^{-1}, *i.e.*, the value at 4.0 Å, which implies that the minimum recombination factor of the polaron states, is only 10^{-18} s^{-1}.

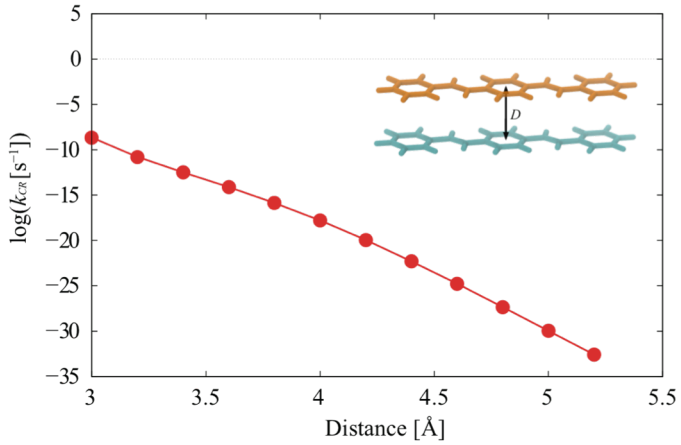

Figure 3-4. Variation of the logarithm of the charge recombination rate with the center-to-center distance of the OPV3 dimer in the face-to-face orientation.

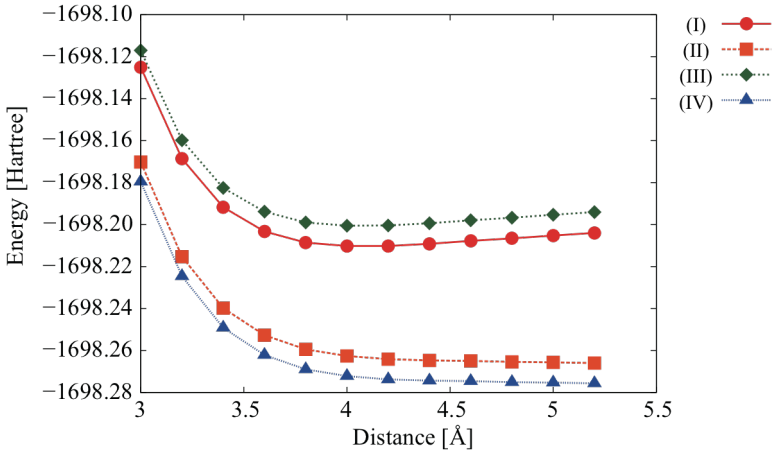

Figure 3-5. Energy variations of the four states (I)-(IV) with the center-to-center distance of the OPV3 dimer in the face-to-face orientation. The minima of the polaron states (I) and (III) occur at 4 Å.

The face-to-face orientation appears to be favorable for the charge recombination reaction because of the large π-π overlap, but such a trend is not indicated by our results. The reason why the face-to-face orientation is not favorable for charge recombination, despite the feasible structure, may be due to the large π-π electrostatic repulsion. The distance of 4.0 Å is too long for sufficient CR to be induced.

3.4.2. Effect of the roll angle

Before giving the results for roll-rotated orientation, we give the results for OPV3-methyl in the crystal structure to clarify the dimer orientations that are suitable for CR. The crystal-structure orientations and the symbols representing them, T1, T2, and P, are shown in Figure 3-6. For the dimer of each orientation extracted from the OPV3-methyl crystal, the charge-recombination rates and Marcus parameters obtained from the CDFT calculations are shown in Table 3-5.

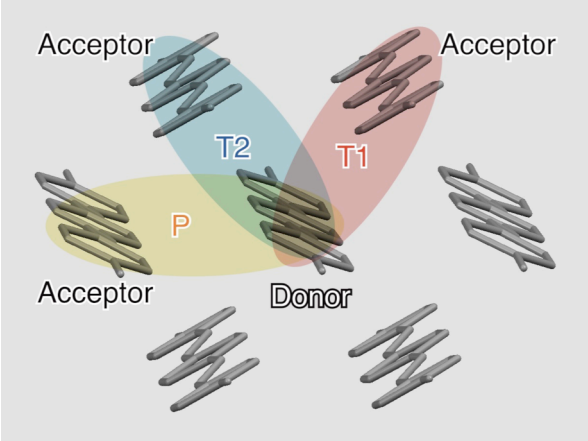

Figure 3-6. Crystal structure of OPV3-methyl. The symbols T1, T2, and P indicate the orientations of the electron transfer channel.

Table 3-5. Calculated Marcus parameters and the decadic logarithm of the charge recombination rate for the dimer of the three orientations in the crystal structure of OPV3-methyl system (Figure 3-6)

Orientation	$-\Delta G^0$	λ	$\Delta G^{\ddagger}$	$\lvert H_{ab}\rvert$	$\log_{10}(k_{CR}[s^{-1}])$
T1-dimer	81.74	24.05	34.60	25.03	9.294
T2-dimer	331.4	26.08	893.6	11.20	~0 (−141.9)
P-dimer	180.4	25.86	230.7	5.266	~0 (−26.43)

Table 3-5 shows that the values of the recombination rate are considerably different

among the orientations. In particular, the largest change among the parameters is the driving force $-\Delta G^0$. Interestingly, the recombination factor of T1-dimer is at least 10^{10} times larger than that of the T2-dimer, although in these orientations the donor and acceptor positions are reversed each other.

We investigated the results for OPV3 from various viewpoints based on the results for OPV3-methyl crystals. We considered the roll rotation of either the donor or acceptor molecule, since the dimer orientations in the OPV3-methyl crystal correspond to the roll rotation by the Euler angle. Table 3-6 shows the charge recombination rate constants and the parameters for various rotation angles, and Figure 3-7 shows the variation of the charge recombination rate constant (on a logarithmic scale) with the rotation angle on the donor and acceptor sides. For the acceptor rotation, the charge recombination rate constant becomes at least 10^7 (= 10^7 $s^{-1}/10^0$ s^{-1}) times larger as the rotation angle increases from 0˚ to 90˚, while for the donor rotation it becomes much smaller with increasing rotation angle. These results indicate that the large tilting of the acceptor causes the recombination rate constant decrease to nearly zero.

Table 3-6. Calculated parameters and the decadic logarithm of the charge recombination rate constant at various roll angles of the acceptor (in the upper part) and of the donor (in the lower part).

Rot. Angle [°]	$\log_{10}(k_{CR}\ [s^{-1}])$	$-\Delta G^0$	λ	$\Delta G^{\ddagger}$	$\lvert H_{ab}\rvert$
Acceptor rotation					
15	~ 0 (−4.32)	133.28	25.33	114.99	43.55
30	−0.47	122.49	25.94	89.84	23.05
45	2.04	111.99	25.84	71.74	10.82
60	0.43	108.47	25.47	67.63	0.73
75	3.82	101.40	25.75	55.56	3.20
90	7.60	93.82	25.98	44.28	25.71
Donor rotation					
15	~ 0 (−24.02)	172.51	24.18	227.46	43.28
30	~ 0 (−51.14)	218.46	24.81	377.90	18.16
45	~ 0 (−93.69)	273.94	25.15	615.39	6.11
60	~ 0 (−126.52)	309.21	25.55	787.20	0.26
75	~ 0 (−156.96)	338.97	25.34	970.39	1.78
90	~ 0 (−182.57)	359.94	25.10	1116.82	1.87

All energies are in kJ mol−1.

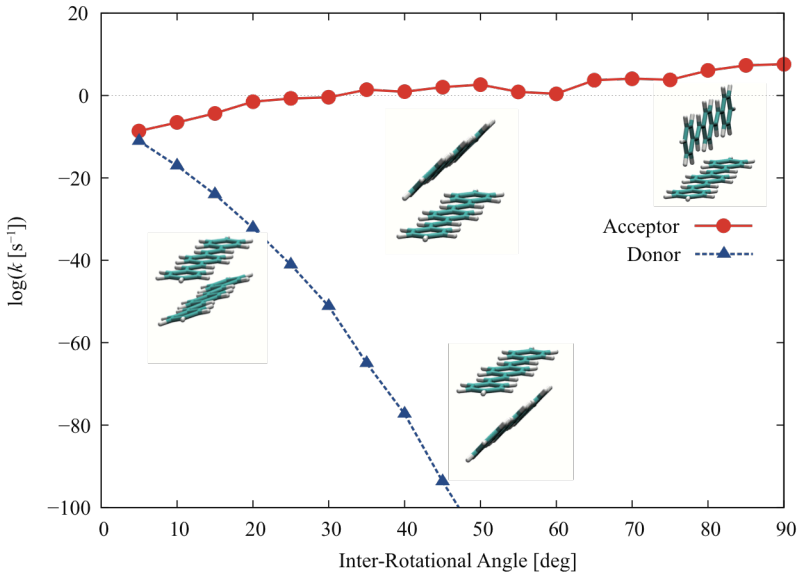

Figure 3-7. Variation of the logarithm of the charge recombination rate constant with the roll angle of the tilted acceptor (red filled circles) and the tilted donor (blue filled triangles) in the OPV3 dimer.

Figure 3-8 shows the energy variations of states (I)-(IV) with the rotation angle of

each side. The energy curves of (II) and (IV) are almost the same for the acceptor and donor rotations, while those of (I) and (III) are considerably different for the acceptor and donor rotations. For the acceptor rotation, the energies of (I) and (III) decrease with increasing angle. In contrast, the (I) and (III) energies increase with increasing angle of donor rotation.

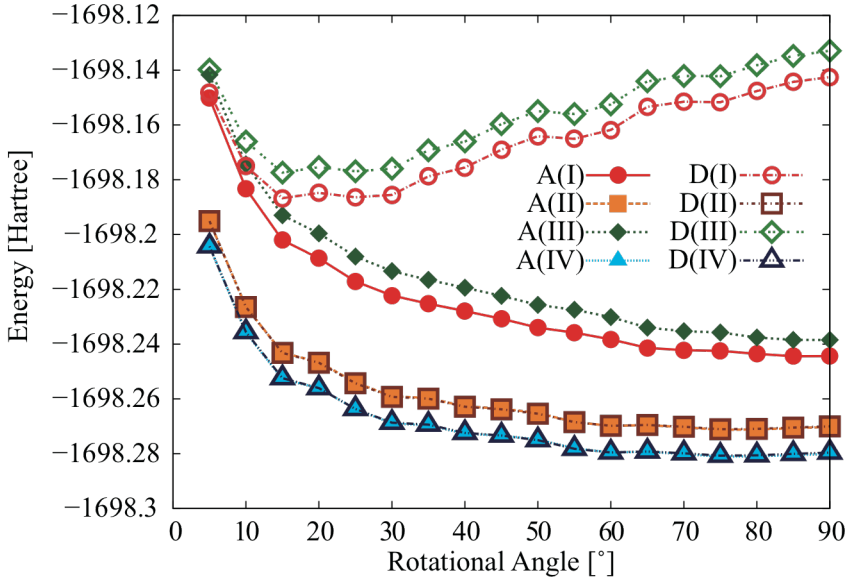

Figure 3-8. Energy variations of the four states of the OPV3 dimer with the roll angle on the acceptor side (filled symbols, A(I)-A(IV)) and the donor side (open symbols, D(I)-D(IV)). The final states (II) and (IV) nearly overlap for the acceptor and donor rotations.

From the energy variations shown in Figure 3-8, the significant angle exceeds 15˚ because for an angle of less than 15˚ the donor-acceptor distance is too short and the system becomes unstable in all the states. In the final states (II) and (IV) with the exciton-pair electronic structure $\{^1D...^3A^*\}$, the two energy curves nearly overlap for the donor and acceptor rotations. On the other hand, the energies of the initial states (I) and (III) with the polaron-pair electronic structure $\{D^{\bullet-}...A^{\bullet+}\}$ become more stable with increasing angle of donor rotation. It is interesting that the energy variations of (I) and

(III) are considerably different for the acceptor rotation and donor rotation.

To explain this behavior of the energy curves in Figure 3-8, the following two reasons are considered. (i) The donor with the rich π-electron density does not face the acceptor plane when the donor molecule rotates. For the rotation of the acceptor molecule, in contrast, the electron-deficient side of the acceptor faces the donor with the rich π-electron density. From this, the rotation of the acceptor is favorable for ET. (ii) The face-to-face orientation (for a rotation of less than 15˚ in Figure 3-8) forms a π-π stacking structure, which can have a large transfer integral; however, the donor and acceptor cannot be close owing to the electron repulsion. The energetic barrier is disadvantageous for ET.

3.4.3. Effect of the intermolecular distance in edge-to-face conformation

To verify the tendency discussed above, we computed the charge recombination rate constant of the OPV3 dimer fixed at a rotation angle of 45˚ and varied the intermolecular distance, *i.e.*, the closest atomic distance between the donor and acceptor (Figure 3-9).

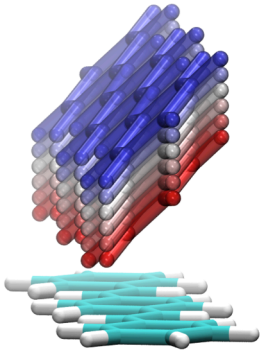

Figure 3-9. One side in the OPV3 dimer is rotated 45˚ and changed intermolecular distance.

The difference in the charge recombination rate constant between the rotated donor and the rotated acceptor is clearly shown in Figure 3-10. The charge recombination rate constant for the acceptor rotation becomes at least 10^6 (=10^6 s^{-1}/10^0 s^{-1}) times larger as the intermolecular distance decreases from 3.5 to 2.7 Å, which can be seen from the comparison of log k_{CR} values at 3.5 to 2.7 Å in the upper part of Table 3-7. Furthermore, we can also see that the large variation of log k_{CR} from 3.5 to 2.7 Å is caused by the variation of the driving force $-\Delta G^0$, which decreases from 148.7 to 97.0 kJ mol^{-1}. On the other hand, the charge recombination rate constant for the donor rotation becomes remarkably smaller with the same change in the intermolecular distance, which can be also checked from log k_{CR} values in the lower part of Table 3-7. As the intermolecular distance decreases, the charge recombination rate constant increases in the tilted acceptor but decreases in the tilted donor.

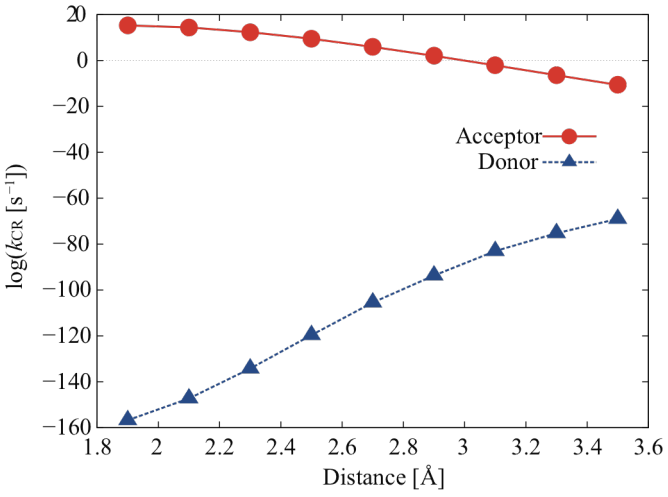

Figure 3-10. Variation of logarithmic of the charge recombination rate constant with the intermolecular distance, i.e., the closest atomic distance between the donor and the acceptor in the OPV3 dimer, where the rotational angle of the acceptor (red filled circles) or the donor (blue filled triangles) is fixed at 45° and the inter molecular distance is varied.

Table 3-7. Calculated charge recombination parameters and the decadic logarighm of the charge recombination rate constant for various closest-contact distances of the acceptor at 45° angle (in the upper part) and the donor at 45° angle (in the lower part) in the OPV3 dimer.

Distance [Å]	$\log_{10}(k_{CR}\ [s^{-1}])$	$-\Delta G^0$	λ	$\Delta G^{\ddagger}$	$\lvert H_{ab}\rvert$
Acceptor rotation					
1.9	15.29	17.98	19.54	0.03	22.31
2.3	12.35	61.44	23.89	14.75	15.40
2.7	5.95	97.00	25.55	49.97	11.94
3.1	−2.13	125.64	26.06	95.11	9.92
3.5	~0 (−10.66)	148.71	26.21	143.10	8.65
Donor rotation					
1.9	~ 0 (−156.74)	347.36	26.20	984.03	36.12
2.3	~ 0 (−134.27)	317.89	25.14	852.42	18.11
2.7	~ 0 (−105.48)	287.79	25.18	684.57	8.90
3.1	~ 0 (−83.07)	261.54	25.25	552.79	4.12
3.5	~ 0 (−69.02)	242.44	25.19	468.35	1.74

All energies are in kJ mol−1.

From the energies of (I)-(IV) shown in Figure 3-11, the energies of (II) and (IV) are similar for the two cases, whereas the energies of (I) and (III) are considerably different. An intermolecular distance of more than 2.7 Å is significant since all the states are unstable when the distance is less than 2.7 Å. Thus, we discuss the recombination rate constants only for the case that intermolecular distance is grater than 2.7 Å. Figure 3-11 shows that the energies of the exciton-pair electron states $\{^1D\ldots{}^3A^*\}$, (II) and (IV), have no significant difference between the cases of acceptor and donor rotation, whereas a large energy difference between the two cases can be seen for the polaron-pair electron states $\{D^{\bullet-}\ldots A^{\bullet+}\}$, (I) and (III). The rotation of the acceptor stabilizes the dimer energy, while that of the donor destabilizes the dimer energy. Generally an anion-cation pair becomes stable as the anion and cation approach each

other. However, the approach of the tilted donor with negative charge (−1) to the positively charged (+1) acceptor causes destabilization. This result confirms that the rotated acceptor can easily approach the donor to within a distance of ~2.7 Å, whereas the rotated donor cannot approach close to the acceptor.

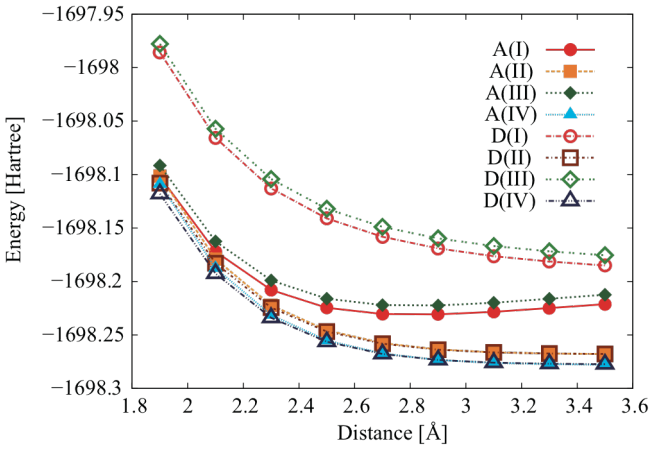

Figure 3-11. Energy variations of (I)-(IV) states of the OPV3 dimer with the intermolecular distance. Two cases are described in the same way as in Figure 3-9; the rotational angle on the acceptor side (filled symbols, A(I)-A(IV)) or the donor side (open symbols, D(I)-D(IV)) is fixed at 45°. The minima of A(I) and A(III) occur at 2.7 Å.

Finally, in the present study, we have not accounted for the dispersion effect, which is important for the intermolecular interaction of the present π-systems. Since the B3LYP functional and the 6-31G(d) basis set used in the present calculations do not suitably evaluate such dispersion effects, we tried to add Grimme's dispersion correction with the present CDFT energies. For Table 3-6, we reexamined the CDFT results including the dispersion correction, which is given in Table 3-8 and found that the dispersion effect in the recombination rate constant is rather minor at the present computational level. However, Grimme's D2 dispersion correction is not sufficiently

worked with middle-size basis sets such as 6-31G(d), and we need a larger basis set added with the advanced dispersion correction such as DFT-D3 to evaluate the intermolecular interaction correctly, which we retain for our future studies.

Table 3-8. logarithm of charge recombination rate constant and four point energies included Grimme's D2 dispersion correction. The dispersion interaction does not make a difference to the charge recombination rate constants because the parameters for Marcus-Hush equation, which is determined by the difference of two energies of four point energies, are almost not changed by the dispersion correction. This is caused by the difference of the dispersion energy between the initial and final structure is small.

Angle [˚]	$\log_{10}(k_{CR}\ [s^{-1}])$	(I)	(II)	(III)	(IV)
A15	−4.13	−1698.33803	−1698.37914	−1698.32908	−1698.38889
A30	−0.30	−1698.34295	−1698.37973	−1698.33412	−1698.38972
A45	2.20	−1698.34591	−1698.37872	−1698.33766	−1698.38869
A60	0.33	−1698.34704	−1698.37967	−1698.33883	−1698.38939
A75	3.97	−1698.35233	−1698.38114	−1698.34578	−1698.39110
A90	7.73	−1698.35579	−1698.38162	−1698.35009	−1698.39168

All energies are in Hartree.

3.5. Conclusions

In the present work, we have investigated the intermolecular triplet-triplet ET of the OPV3 dimer as a model system for the PPV charge recombination process by using CDFT. In addition, we analyzed the relation between the intermolecular orientation of the dimer and the recombination rate constant to provide guidelines for the molecular design of effective charge recombination systems. It was found that the face-to-face orientation has a low recombination rate constant of 10^{-18} s^{-1} at an intermolecular distance of 4.0 Å, where the polaron states (I) and (III) have energy minima. The value of 10^{-18} s^{-1} for the face-to-face orientation is much lower than that of 10^{6} s^{-1} for the edge-to-face orientation at an intermolecular distance of 2.7 Å with 45˚ rotation of the

acceptor.

In the edge-to-face case, the roll rotation of the donor molecular causes the charge recombination rate constant to decrease to nearly zero, whereas that of the acceptor molecule increases the recombination rate constant tot the order 10 s^{-1}. Regarding the energies of the four states, those of the final exciton-pair states (II) and (IV) are almost the same for both donor rotation and acceptor rotation, whereas for the initial polaron-pair states (I) and (III), the energies of the acceptor rotation become much lower than those of the donor rotation with increasing angle of rotation. This induces a large difference in the driving force $-\Delta G^0$ between the two cases, which ultimately causes the difference in the recombination rate constants.

We carried out the calculation for the dimer with several intermolecular distances and a fixed rotation angle (45˚) to investigate how the difference between the tilted molecules occurs. The approach of the tilted donor to the flat acceptor decreases the recombination rate constant, while the approach of the tilted acceptor to the flat donor increases the recombination rate constant. The polaron states become stable in the former case (at least down to an intermolecular distance of 2.7 Å), while they become unstable in the latter case. From the results, we can conclude that the flat donor and tilted acceptor pair is a more favorable orientation for triplet-triplet charge recombination then the tilted-donor and flat acceptor pair.

The present computational results show that the molecular orientation is a very important factor for material design, and suggests that single crystals with herringbone structure such as rubrene and tetracene have higher hole-mobility than those with a

lamella structure with large transfer integrals.

The present results would also be helpful for readers of supramolecular chemistry and related fields. For example, orientation and organization of *p*-phenylenevinylene derivatives have been paid much attention. In some cases, orientation and arrangements of the component chromophores are highly controlled and modified. It is noted that the methyl-substituted system, OPV3-methyl, has a larger value in the charge recombination rate constant than the non-substituted OPV3 as shown in Table 3-3. This suggests a possibility that the OPV3 derivatives with various functional groups have a large charge recombination rate constant. The OPV3 derivatives and the conjugate length effects are discussed in Chapter 4.

4. Effect of Conjugation length or Sidechains for Charge Recombination in Poly(para-phenylenevinylene)

4.1. Introduction

Organic semiconductors have received much attention in many fields because of their utility and wide applicability to various devices. Especially, organic light-emitting diodes (OLEDs) are better than other light-emitting diodes in terms of cost and flexibility. However, the performance of OLEDs has not been good enough for use in some devices [86]. The luminescence process of poly(*para*-phenylenevinylene) (PPV) as an OLED material is as follows: (1) injection of positive or negative charges from the electrode; (2) collapse of the positive or negative charge, resulting in excitement by charge recombination; (3) from the excited chromophore (A^*) photons are emitted (same as Figure 3-1 in Section 3.1).

Although charge recombination in PPV before luminescence is important among these processes, it has so far been difficult to observe such a process. This is why theoretical insight is necessary to investigate the process. In addition, it has been reported that the morphology of PPV changes by side-chain modification [87]. The electroluminescence quantum yields of PPV are different from those of PPV derivatives whose side-chains are modified, *e.g.*, OC1C10-PPV and MEH-PPV [52,55]. In our previous study, we found that the orientation of the molecules improved charge recombination, and suggested PPV modified side-chain to change the orientation [37]. Accordingly, we investigated the effect of PPV side-chains in order to further

understand these compounds and to design new types of OLEDs. In this thesis, I focus on the effect of the conjugation length and/or the presence of side-chains on the intermolecular charge recombination process by computing the rate constant of these molecules.

4.2. Models and Methods

4.2.1. Models

We used two models to understand these effects, as shown in Scheme 4-1 and Scheme 4-2. First, we employed the *n*-mer model of oligo-*para*phenylenevinylene (OPV*n*) as a model for PPV to investigate the effects of conjugation length. In the first stage of this study, we used three molecules from $n = 2$ (OPV2) to $n = 4$ (OPV4). Next, we investigated the OPV3 derivatives OPV3-methyl (Scheme 4-1b) and OPV3-vinyl (Scheme 4-1c), terminating the OPV3 molecules with a methyl group or vinyl group. As for the other model, in order to investigate the substituent effect, we used the OPV3 derivatives O(PV-OEt)3, O(PV-CN)3, and O(PV-F)3, in which the hydrogen atom at the ortho- position in each unit is replaced with an ethoxy group, a cyano group, and fluorine atoms, respectively (Scheme 4-2).

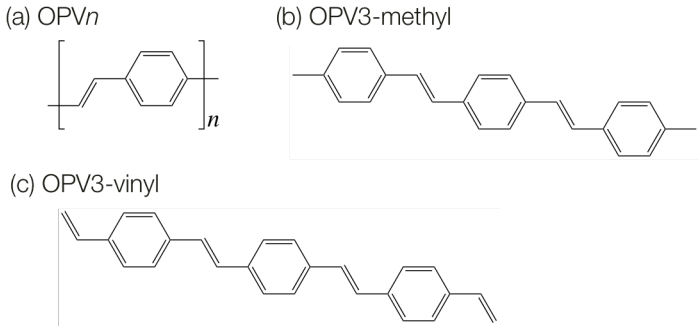

Scheme 4-1

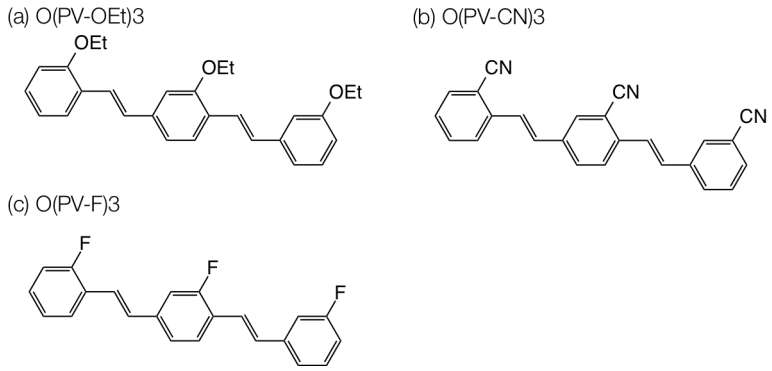

Scheme 4-2

We used the "dimer system", which consists of two molecules, donor and acceptor molecules. The initial state is the charge-separated state ($D^{\bullet-}\ldots A^{\bullet+}$) and the final state is the exciton state ($D\ldots {}^3A^*$) (see also Figure 3-1). The structures of molecules used for the dimers were defined from the geometry of the optimized structures of the monomers ($D^{\bullet-}$, $A^{\bullet+}$, D, ${}^3A^*$). As shown in Figure 4-1, we used a stacked model whose distances were 4.0 Å because we found in our previous work [37] it is the most stabilized distance for OPV3, also Shuai *et al.* have used 4.0 Å in their works [79,81]. In addition, we calculated the inversed dimer for side-chain systems (Figure 4-2).

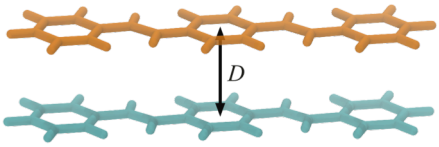

Figure 4-1. Cofacial-stacked dimer model of OPV3. In this work, D = 4.0 Å.

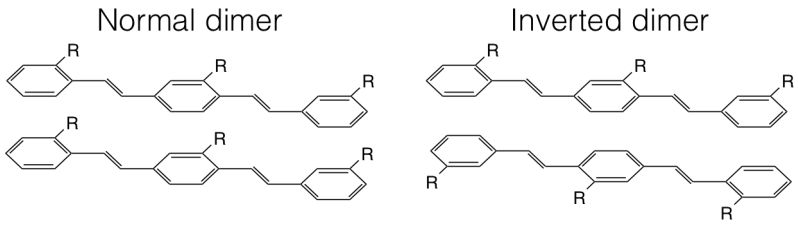

Figure 4-2. Normal and inverted dimers for side-chain systems.

4.2.2. Computational methods

To calculate the electronic states before and after the charge recombination process, we used constrained density functional theory (CDFT) [26,29,85]. CDFT enables us to calculate the system-delocalized charge or spin density, *i.e.*, the charge-separated state and the different spin states between the fragments. Moreover, CDFT can obtain the coupling matrix element with good accuracy [28,34].

We calculated the initial and final electronic states for the "dimer system" using CDFT, which enabled us to estimate the charge- or spin-localized system. CDFT imposes constraints on the charge or spin density of arbitrary molecular fragments. In this study, the difference in the charge density between the anionic donor and cationic acceptor molecules for the initial state was set to 2.0, and the difference of the spin density between the neutral donor and excited acceptor molecules for the final state was

set to −2.0.

4.2.3. Estimating Marcus parameters

By using CDFT, we estimated the driving force, $-\Delta G^0$, the reorganization energy, l, and the activation energy, $\Delta G^{\ddagger}$, using the four-point method [39].

The four-point energies were calculated from the dimer structures and the electronic states for the initial and final states. We plugged those parameters in the Marcus–Hush equation [72,88]. With equations (2.32)–(2.35), we can predict a recombination rate. The details are shown in our previous study [37].

4.3. Computational Details

The geometries of all monomers were optimized at the B3LYP/6-31G(d) level with the Gaussian 09 package [89]. In calculating the dimer, we performed CDFT with a program [90] developed in our laboratory at the same level of theory. In addition, we estimated the van der Waals interaction by B3LYP-D2 [91].

4.4. Results and Discussion

The results for the conjugation length dependencies are shown in Table 4-1 and Table 4-2. The recombination rate is more than 10^{10} larger with increasing numbers of phenylenevinylene units. The terminal substituents (methyl or vinyl group) increase the recombination rate as compared to the unmodified OPV3. The largest contributing parameter is the driving force, where that for OPV3 was 70 kJ mol^{-1} larger than that for OPV2. On the other hand, the reorganization energy and the coupling matrix element are not much different from the driving force for the conjugation length. In the initial

electronic state, the anion and the cation attract each other because of the electrostatic interaction. If the conjugation length increases, the electrostatic interaction decreases because the charge density is spread throughout the molecule. In fact, the difference between the summation of the monomer energies and the dimer energy (the stabilization energy by dimerization, *i.e.*, −(dimerization energy); shown in Table 4-2) decreases with increasing conjugation length. On the other hand, in the final electronic state, the interaction between the molecular orbitals is dominant because the electrostatic attractive force is very weak. Then, the stabilization from the dimerization increases with increasing conjugation length because of the spread of π-orbitals.

Table 4-1. Summary for conjugation length versus computed Marcus parameters and the logarithm of charge recombination rate constants.

System	$\log_{10}(k_{CR}\ [s^{-1}])$	$-\Delta G^0$	λ	$\Delta G^{\ddagger}$	$\lvert H_{ab}\rvert$
OPV2	−38.51	228.2	31.59	305.8	19.33
OPV3	−17.81	162.8	25.15	188.0	19.40
OPV4	−6.25	134.6	24.71	122.0	19.33
OPV3-methyl	−13.45	155.7	25.82	163.3	20.44
OPV3-vinyl	−8.98	140.9	24.57	137.6	19.42

All energies are in kJ mol^{-1}.

Table 4-2. Summary for conjugation length versus dimerization energy and properties, *i.e.* driving force $-\Delta G^0$, ionic potential, electron affinity, excitation energy, at monomer level.

System	Dimerization energy		Monomer $-\Delta G^0$	IP	EA	E_x
	Initial structure	Final structure				
OPV2	−238.4	9.7	469.6	693.4	−41.21	202.2
OPV3	−191.7	15.1	369.4	632.1	−102.5	171.5
OPV4	−162.2	20.8	317.5	600.8	−134.6	158.0
OPV3-methyl	−186.2	18.0	359.9	613.2	−93.57	170.5
OPV3-vinyl	−171.4	17.4	329.7	611.2	−132.8	160.0

All energies are in kJ mol^{-1}.

If the dimerization energy is dominant for $-\Delta G^0$, ΔG^0 will decrease with increasing conjugation length. However, the current results show the reverse trend, which implies the other effect surpassing the intermolecular interaction. In addition, the conjugation length decreases the monomer $-\Delta G^0$ value, which was calculated from the sum of monomer energies. Note that the dimerization energy is significant because the rate constant increases as the value ($\Delta G^0 + \lambda$) decreases.

For further investigation, we present the ionization potential (IP), the electron affinity (EA), and the excitation energy (E_x) for each model at the monomer level in Table 4-2. 6-31+G(d) basis set is used in these calculations. In computing the monomer properties, we employed the adiabatic IP/EA and the difference between the triplet and the ground-state energy for E_x. As the conjugated length increases (*n* increases), IP of OPV*n* decreases because the highest occupied molecular orbital (HOMO) level is stabilized. Similarly, EA and E_x are stabilized because the HOMO–lowest unoccupied molecular (LUMO) gaps decreases. In particular, the sum of IP and EA (*i.e.*, the

contribution of the initial state for monomer $-\Delta G^0$) plays a significant role in controlling the value of $-\Delta G^0$. IP and EA decrease by ~50 kJ mol^{-1} with increasing conjugation length and Ex decreases by ~20 kJ mol^{-1} with increasing conjugation length. Therefore, because the monomer $-\Delta G^0$ equals E_x − (IP + EA), the sum of IP and EA contributes the most to $-\Delta G^0$.

The results of the effects of the side-chains are shown in Table 4-3. The recombination rate constants for each OPV3 derivative-modified side-chain are greater than that of the unmodified OPV3. Similarly, an experimental report on the charge recombination between cyano-anthracenes and *N*, *N*-dimethyl aniline with femtosecond time-resolved fluorescence measurements showed that mono-cyano-anthracenes have a longer mean lifetime for charge recombination than di-, tri-, and tetra-cyano-anthracene [92]. The OPV3 derivative-modified ethoxy group, which is an electron donor and steric substituent, is the easiest to recombine. On the other hand, although the electron-attracting side-chains O(PV-CN)3 and O(PV-F)3 have larger rate constants, k_{CR}, than OPV3, they have smaller k_{CR} on the order of 10^7–10^{10} compared to O(PV-OEt)3.

Table 4-3. Driving force $-\Delta G^0$, reorganization energy λ, activity energy $\Delta G^{\ddagger}$, coupling matrix element H_{ab}, and logarithm of the rate constant $\log_{10}(k_{CR})$ for OPV3 derivative-modified side-chains and inverted dimers.

System	$-\Delta G^0$	λ	$\Delta G^{\ddagger}$	$\lvert H_{ab}\rvert$	$\log_{10}(k_{CR}\ [s^{-1}])$
OPV3	162.8	25.15	188.0	19.40	−17.81
O(PV-OEt)3	146.2	29.73	114.0	23.21	−4.74
O(PV-CN)3	155.9	26.98	153.9	18.63	−11.89
O(PV-F)3	161.1	27.05	166.1	19.24	−14.00
Inverted O(PV-OEt)3	150.3	30.05	120.2	20.38	−5.94
Inverted O(PV-CN)3	156.6	27.08	154.9	18.94	−12.05
Inverted O(PV-F)3	161.2	27.07	166.3	20.11	−13.99

All energies in kJ mol^{-1}.

The coupling matrix element H_{ab} increases due to the electron-donating side-chain because the p-orbitals are extended by the electron donation to the backbone of OPV3. On the other hand, H_{ab} decreases by the electron-attracting side-chains because they draw electrons from the backbone of OPV3. Table 4-4 and Figure 4-3 show the sum of the Becke charge of the atoms in the backbone, excluding the carbon atom-bonded side-chains, and the electrostatic potentials, respectively, for each OPV3 derivative.

Table 4-4. Backbone charge in each side-chain group

System	Backbone charge
OPV3	−0.028
O(PV-OEt)3	−0.059
O(PV-CN)3	0.625
O(PV-F)3	0.128

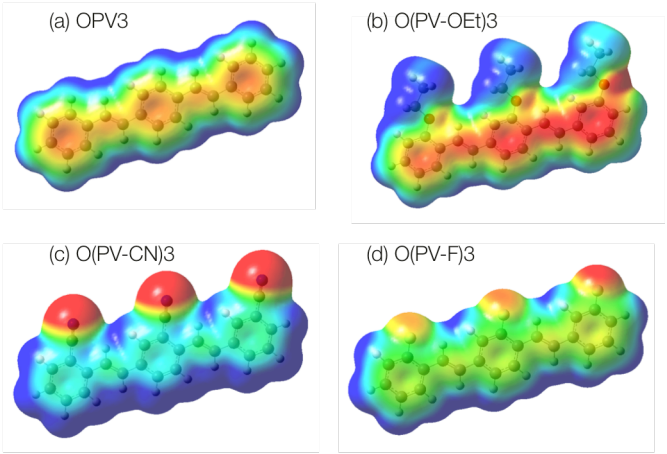

Figure 4-3. Electrostatic potential with a scale 0.025–0.015.

The $-\Delta G^0$ values of the OPV3 derivatives with side-chains are larger than that of OPV3 because of the steric bulk of the side-chains. When the positions of the side-chains are inverted between each monomer (see Figure 4-2), the recombination rate constants are similar to or smaller than that of the non-inverted dimer. The H_{ab} value of O(PV-OEt)3 is smaller and the H_{ab} values of O(PV-CN)3 and O(PV-F)3 are slightly larger than the H_{ab} value of the non-inverted dimer. This result suggests that the effects of the side-chains intensify when the side-chains are in the same direction. In addition, the driving force $-\Delta G^0$ of the inverted dimer is similar to or larger than that of the non-inverted dimer. This is because the repulsion of the partial charge of the side-chain decreases with increasing distance between the side-chains.

4.5. Conclusions

We have investigated the effects of the conjugation length and the presence of side-chains on the recombination process of PPV in this study. The recombination rate

constants increased with increasing conjugation length of PPV because of the change of the driving force, $-\Delta G^0$. Stabilization by dimerization decreased the $-\Delta G^0$ and ($\Delta G^0 + \lambda$) values; however, the properties of the monomer had a significant effect on conjugation length. In particular, the change of the ionization potential and the electron affinity for the conjugation length had the largest effect on the driving forces. The OPV3 derivatives modified by side-chains, that is, ethoxy cyano groups and fluorine atoms, all exhibited larger rate constants than the original OPV3. O(PV-OEt)3 exhibited the largest rate constant, followed by O(PV-CN)3 and O(PV-F)3. The coupling matrix element H_{ab} was affected by the electron-donation effect of the side-chains. $-\Delta G^0$ was affected by the steric bulk of the side-chains. We found that the conjugation length and substituents with electron-donating bulky side-chains are important for developing preferable materials for OLEDs using PPV derivatives.

5. General Conclusions

We studied the effects of (1) the orientation, (2) conjugation length, and (3) derivatives on the charge-recombination process of the organic lit-emitting diode OPV3.

In Chapter 3, we investigated the effect of the orientation of OPV3 on the charge-recombination process. In this process, charge transfer between a negative charged donor molecule and the positive charged acceptor molecule ($D^{\bullet -}\ldots A^{\bullet +}$) results in recombination to the ground state and the excited state ($D\ldots A^{*}$). Computations were performed for the dimer systems, combining the donor and acceptor molecules, in the initial and final electronic states and structures. In addition, the donor or acceptor of the molecule in the dimer was rotated along the chain direction axis to investigate the orientation effect. We found that rotation causes a drastic change in the charge recombination process. Rotation of the donor makes charge recombination difficult, whereas acceptor rotation facilitates recombination. We concluded that this is caused by two factors related to the π-electron in the donor and acceptor. The first reason is that the donor electron is able to move to the acceptor molecule because the π-electron in the donor molecule faces the tilted acceptor molecule. The second reason is that the electron repulsion between the π-electron of the donor and the acceptor is decreased due to the rotation.

In Chapter 4, we investigated the effect of the conjugation length and several side chains on the charge-recombination process for OPV. In this study, the conjugation length varied between 2−4 units of OPV; the investigated OPV3 derivatives are

OPV3-methyl, OPV3-vinyl, O(PV-OEt)3, O(PV-CN)3, and O(PV-F)3. Note that in the OPV3-methyl and OPV3-vinyl species, the OPV3 molecule is terminated with a methyl group or a vinyl group, whereas O(PV-OEt)3, O(PV-CN)3, and O(PV-F)3 have an ethoxy group, a cyano group, and fluorine atoms at the *ortho*-position of OPV3, respectively. The recombination-rate constant increases with an increase of the conjugation length of OPV because the driving force decreases due to a decrease of the sum of the IP and EA. End-group terminated OPV3 shows a trend commensurate with the conjugation length of OPV. Because OPV3-methyl does not have increased conjugation length, whereas the conjugation length is increased for OPV3-vinyl, OPV3-vinyl has a larger recombination-rate constant than OPV3-methyl. Investigation of the side chain effect showed that O(PV-OEt)3 has the largest rate constant followed by O(PV-CN)3 and O(PV-F)3 in succession. The largest rate constant of O(PV-OEt)3 is attributed to the increase of the coupling matrix element by the electron-donating, bulky side chain. The electron-donating side confers high electron density to the OPV3 backbone.

This thesis describes the factors influencing the charge-recombination process affecting the luminescence process of PPV OLEDs. The study suggests an effective method for material design for OLEDs and is expected to promote the development of efficient OLEDs.

6. References

[1] Y. Yamashita, Sci. Technol. Adv. Mater. **10**, 24313 (2009).

[2] V. Coropceanu, J. Cornil, D. A. da Silva Filho, Y. Olivier, R. Silbey, and J.-L. Brédas, Chem. Rev. **107**, 926 (2007).

[3] C. Wang, H. Dong, W. Hu, Y. Liu, and D. Zhu, Chem. Rev. **112**, 2208 (2012).

[4] S. Günes, H. Neugebauer, and N. S. Sariciftci, Chem. Rev. **107**, 1324 (2007).

[5] F. C. Grozema, P. T. van Duijnen, Y. a. Berlin, M. a. Ratner, and L. D. a. Siebbeles, J. Phys. Chem. B **106**, 7791 (2002).

[6] H. Dong, X. Fu, J. Liu, Z. Wang, and W. Hu, Adv. Mater. **25**, n/a (2013).

[7] S. Watanabe, Y. Shimodo, and K. Morihashi, Theor. Chem. Acc. **130**, 807 (2011).

[8] L. Wang, G. Nan, X. Yang, Q. Peng, Q. Li, and Z. Shuai, Chem. Soc. Rev. **39**, 423 (2010).

[9] Y. Mei, D. M. Sherman, W. Liu, and J. Brugger, Geochim. Cosmochim. Acta **102**, 45 (2013).

[10] M. Segal, M. Baldo, R. Holmes, S. Forrest, and Z. Soos, Phys. Rev. B **68**, 75211 (2003).

[11] B. Milián-Medina and J. Gierschner, Org. Electron. **13**, 985 (2012).

[12] O. Nuyken, S. Jungermann, V. Wiederhirn, E. Bacher, and K. Meerholz, Monatshefte Für Chemie - Chem. Mon. **137**, 811 (2006).

[13] W. J. Baker, T. L. Keevers, J. M. Lupton, D. R. McCamey, and C. Boehme, Phys. Rev. Lett. **108**, 267601 (2012).

[14] S. Yeganeh and T. V. Voorhis, J. Phys. Chem. C 20756 (2010).

[15] Z. Shuai and Q. Peng, Phys. Rep. **537**, 123 (2014).

[16] H. Nakanotani, T. Higuchi, T. Furukawa, K. Masui, K. Morimoto, M. Numata, H. Tanaka, Y. Sagara, T. Yasuda, and C. Adachi, Nat. Commun. **5**, 4016 (2014).

[17] G. G. Malliaras and J. C. Scott, J. Appl. Phys. **83**, 5399 (1998).

[18] Y. Tao, Q. Wang, L. Ao, C. Zhong, C. Yang, J. Qin, and D. Ma, J. Phys. Chem. C 601 (2010).

[19] M. Wohlgenannt, K. Tandon, S. Mazumdar, and S. Ramasesha, Nature **409**, 494 (2001).

[20] T. Ogiwara, Y. Wakikawa, and T. Ikoma, J. Phys. Chem. A (2015).

[21] N. Matsumoto and C. Adachi, J. Phys. Chem. C **114**, 4652 (2010).

[22] D. Yokoyama, J. Mater. Chem. **21**, 19187 (2011).

[23] J. Li, H. Nomura, H. Miyazaki, and C. Adachi, Chem. Commun. (Camb). **50**, 6174 (2014).

[24] S. Difley, D. Beljonne, and T. Van Voorhis, J. Am. Chem. Soc. **130**, 3420 (2008).

[25] Q. Wu and T. Van Voorhis, J. Chem. Theory Comput. **2**, 765 (2006).

[26] Q. Wu and T. Van Voorhis, Phys. Rev. A **72**, 24502 (2005).

[27] Q. Wu, C.-L. Cheng, and T. Van Voorhis, J. Chem. Phys. **127**, 164119 (2007).

[28] Q. Wu and T. Van Voorhis, J. Chem. Phys. **125**, 164105 (2006).

[29] B. Kaduk, T. Kowalczyk, and T. Van Voorhis, Chem. Rev. **112**, 321 (2012).

[30] B. Kaduk, T. Tsuchimochi, and T. Van Voorhis, J. Chem. Phys. **140**, 18A503 (2014).

[31] H. S. Ren, M. J. Ming, J. Y. Ma, and X. Y. Li, J. Phys. Chem. A **117**, 8017 (2013).

[32] A. de la Lande and D. R. Salahub, J. Mol. Struct. THEOCHEM **943**, 115 (2010).

[33] T. Kowalczyk, L.-P. Wang, and T. Van Voorhis, J. Phys. Chem. B **115**, 12135 (2011).

[34] A. Kubas, F. Hoffmann, A. Heck, H. Oberhofer, M. Elstner, and J. Blumberger, J. Chem. Phys. **140**, 104105 (2014).

[35] D. Casanova, J. Chem. Theory Comput. **10**, 324 (2013).

[36] H. Wang, Y. Liu, M. Li, H. Huang, H. M. Xu, R. J. Hong, and H. Shen, Optoelectron. Adv. Mater. Rapid Commun. **4**, 1166 (2010).

[37] K. Aikawa, M. Sumita, Y. Shimodo, and K. Morihashi, Phys. Chem. Chem. Phys. **17**, 20923 (2015).

[38] Y. Shimodo, K. Morihashi, and T. Nakano, Theochem **770**, 163 (2006).

[39] S. F. Nelsen, S. C. Blackstock, and Y. Kim, J. Am. Chem. Soc. **109**, 677 (1987).

[40] D. J. Choo, A. Talaie, Y. K. Lee, J. Jang, S. H. Park, G. Huh, K. H. Yoo, and J. Y. Lee, **363**, 37 (2006).

[41] W. Geens, S. E. Shaheen, B. Wessling, C. J. Brabec, J. Poortmans, and N. Serdar Sariciftci, Org. Electron. **3**, 105 (2002).

[42] S. Tretiak, a. Saxena, R. L. Martin, and a. R. Bishop, J. Phys. Chem. B **104**, 7029 (2000).

[43] R. Marks and J. Halls, J. Phys. Condens. Matter **6**, 1379 (1994).

[44] T. Yasuda, M. Saito, H. Nakamura, and T. Tsutsui, Chem. Phys. Lett. **452**, 110 (2008).

[45] P. W. M. Blom and M. C. J. M. Vissenberg, Mater. Sci. Eng. Reports **27**, 53 (2000).

[46] N. Vilbrandt, A. Gassmann, H. von Seggern, and M. Rehahn, Macromolecules acs. macromol.5b01249 (2016).

[47] S. Barth, H. Bässler, T. Wehrmeister, and K. Müllen, J. Chem. Phys. **106**, 321 (1997).

[48] H. Nakanotani, M. Saito, H. Nakamura, and C. Adachi, Appl. Phys. Lett. **95**, 33308 (2009).

[49] P. W. M. Blom and M. C. J. M. Vissenberg, Mater. Sci. Eng. Reports **27**, 53 (2000).

[50] S. H. Chen, A. C. Su, and H. L. Chou, Macromolecules **37**, 167 (2004).

[51] D. Comoretto, G. Dellepiane, and F. Marabelli, Phys. Rev. B **62**, 173 (2000).

[52] D. Braun, E. G. J. Staring, R. C. J. E. Demandt, G. L. J. Rikken, Y. A. R. R. Kessener, and A. H. J. Venhuizen, Synth. Met. **66**, 75 (1994).

[53] D. D. C. Bradley, J. Phys. D. Appl. Phys. **20**, 1389 (1987).

[54] S. Suramitr, T. Kerdcharoen, T. Srikhirin, and S. Hannongbua, Synth. Met. **155**, 27 (2005).

[55] Y. Cao, I. Parker, G. Yu, C. Zhang, and A. Heeger, Nature **397**, 414 (1999).

[56] L. H. Thomas, Proc. Camb. Philol. Soc. **23**, 542 (1927).

[57] E. Fermi, Rend. Accad. Naz. Lincei. **6**, 602 (1927).

[58] P. A. M. Dirac, Proc. Cambridge Philos. Soc. **26**, 376 (1930).

[59] P. Hohenberg and W. Kohn, Phys. Rev. B **136**, 864 (1964).

[60] W. Kohn and L. Sham, Phys. Rev. A **140**, 1133 (1965).

[61] J. A. Pople, R. Seeger, and R. Krishnan, Int. J. Quantum Chem. **11**, 149 (1977).

[62] R. G. Parr and W. Yang, *Density-Functional Theory of Atoms and Molecules* (Oxford Press, 1989).

[63] A. D. Becke, J. Chem. Phys. **140**, 18A301 (2014).

[64] A. D. Becke, J. Chem. Phys. **98**, 5648 (1993).

[65] M. Lundberg and P. E. M. Siegbahn, J. Chem. Phys. **122**, 224103 (2005).

[66] J. Perdew and A. Zunger, Phys. Rev. B **23**, 5048 (1981).

[67] V. Anisimov, J. Zaanen, and O. Andersen, Phys. Rev. B **44**, 943 (1991).

[68] H. Iikura, T. Tsuneda, T. Yanai, and K. Hirao, J. Chem. Phys. **115**, 3540 (2001).

[69] R. S. Mulliken, J. Chem. Phys. **23**, 1833 (1955).

[70] P.-O. Löwdin, J. Chem. Phys. **18**, 365 (1950).

[71] A. D. Becke, J. Chem. Phys. **88**, 2547 (1988).

[72] R. A. Marcus, J. Chem. Phys. **24**, 966 (1956).

[73] J. R. Miller, L. T. Calcaterra, and G. L. Closs, J. Am. Chem. Soc. **106**, 3047 (1984).

[74] A. Inigo, H.-C. Chiu, W. Fann, Y.-S. Huang, U.-S. Jeng, T.-L. Lin, C.-H. Hsu, K.-Y. Peng, and S.-A. Chen, Phys. Rev. B **69**, 75201 (2004).

[75] E. H. a Beckers, S. C. J. Meskers, A. P. H. J. Schenning, Z. Chen, F. Würthner, P. Marsal, D. Beljonne, J. Cornil, and R. a J. Janssen, J. Am. Chem. Soc. **128**, 649 (2006).

[76] M. D. Curtis, J. Cao, and J. W. Kampf, J. Am. Chem. Soc. **126**, 4318 (2004).

[77] V. C. Sundar, J. Zaumseil, V. Podzorov, E. Menard, R. L. Willett, T. Someya, M. E. Gershenson, and J. a Rogers, Science **303**, 1644 (2004).

[78] U. Sondermann, A. Kutoglu, and H. Bässler, J. Phys. Chem. **89**, 1735 (1985).

[79] Z. Shuai, D. Beljonne, R. Silbey, and J.-L. Brédas, Phys. Rev. Lett. **84**, 131 (2000).

[80] M. Ottonelli, D. Duce, S. Thea, and G. Dellepiane, J. Nanosci. Nanotechnol.

13, 5186 (2013).

[81] D. Beljonne, A. Ye, Z. Shuai, and J.-L. Brédas, Adv. Funct. Mater. **14**, 684 (2004).

[82] J.-L. Brédas, D. Beljonne, V. Coropceanu, and J. Cornil, Chem. Rev. **104**, 4971 (2004).

[83] T. Granier, E. L. Thomas, D. R. Gagnon, F. E. Karasz, and R. W. Lenz, J. Polym. Sci. B **24**, 2793 (1986).

[84] U. Jeng, C.-H. Hsu, H.-S. Sheu, H.-Y. Lee, A. R. Inigo, H. C. Chiu, W. S. Fann, S. H. Chen, A. C. Su, T.-L. Lin, K. Y. Peng, and S. A. Chen, Macromolecules **38**, 6566 (2005).

[85] Q. Wu and T. Van Voorhis, J. Phys. Chem. A **110**, 9212 (2006).

[86] D. Braun and A. J. Heeger, Appl. Phys. Lett. **58**, 1982 (1991).

[87] M. Kemerink, J. K. J. van Duren, A. J. J. M. van Breemen, J. Wildeman, M. M. Wienk, P. W. M. Blom, H. F. M. Schoo, and R. A. J. Janssen, Macromolecules **38**, 7784 (2005).

[88] N. S. Hush, J. Chem. Phys. **28**, 962 (1958).

[89] M. J. Frisch, G. W. Trucks, H. B. Schlegel, G. E. Scuseria, M. A. Robb, J. R. Cheeseman, G. Scalmani, V. Barone, B. Mennucci, G. A. Petersson, H. Nakatsuji, M. Caricato, X. Li, H. P. Hratchian, A. F. Izmaylov, J. Bloino, G. Zheng, J. L. Sonnenberg, M. Hada, M. Ehara, K. Toyota, R. Fukuda, J. Hasegawa, M. Ishida, T. Nakajima, Y. Honda, O. Kitao, H. Nakai, T. Vreven, J. Montgomery, J. A., J. E. Peralta, F. Ogliaro, M. Bearpark, J. J. Heyd, E. Brothers, K. N. Kudin, V. N. Staroverov, R. Kobayashi, J. Normand, K. Raghavachari, A. Rendell, J. C. Burant, S. S. Iyengar, J. Tomasi, M. Cossi, N. Rega, N. J. Millam, M. Klene, J. E. Knox, J. B. Cross, V. Bakken, C. Adamo, J. Jaramillo, R. Gomperts, R. E. Stratmann, O. Yazyev, A. J. Austin, R. Cammi, C. Pomelli, J. W. Ochterski, R. L. Martin, K. Morokuma, V. G. Zakrzewski, G. A. Voth, P. Salvador, J. J. Dannenberg, S. Dapprich, A. D. Daniels, Ö. Farkas, J. B. Foresman, J. V. Ortiz, J. Cioslowski, and D. J. Fox, (2009).

[90] T. Ogawa, M. Sumita, Y. Shimodo, and K. Morihashi, Chem. Phys. Lett. **511**, 219 (2011).

[91] S. Grimme, J. Comput. Chem. **27**, 1787 (2006).

[92] A. Rosspeintner, G. Angulo, and E. Vauthey, J. Phys. Chem. A **116**, 9473

(2012).

Publication List

Main papers

K. Aikawa, M. Sumita, Y. Shimodo, and K. Morihashi, *Phys. Chem. Chem. Phys.* **17**, 20923 (2015).

K. Aikawa, T. Matsui, and K. Morihashi, *Chem. Lett.* **45**, 628 (2016).

Others

K. Sodeyama, Y. Yamada, K. Aikawa, A. Yamada, and Y. Tateyama, J. Phys. Chem. C **118**, 14091 (2014).

Y. Tateyama, M. Sumita, Y. Ootani, K. Aikawa, R. Jono, L. Han, and K. Sodeyama, J. Phys. Chem. C **118**, 16863 (2014).

Acknowledgments

This Ph.D. study would not have been possible to do without the support and guidance that I received from many people.

Firstly, I would like to express my sincere gratitude to my advisor Prof. Kenji Morihashi for the support of my Ph.D. study and this thesis. I have learned the essence of the computational chemistry through his guidance. Also, he has provided me with enough computational resources for my work and experimental computation. I would like to thank Prof. Tatsuro Arai, Prof. Kazuya Saito, and Prof. Takaaki Ishibashi for incisive comments as the deputy examiner of my thesis.

I also would like to thank Associate Prof. Toru Matsui for the support of our paper and this thesis. His great support helped me since I have left from the University. I would like to thank Norio Tomotsu for the valuable advice and supplying crystal data of OPV3-methyl. I want to thank Dr. Masato Sumita for the support writing our paper. Dr. Yasuyo Shimodo made an enormous contribution to the program developed in the Morihashi Laboratory.

I would like to thank the members of Nano-System Computational Science group in National Institute for Materials Science (NIMS). I have studied many things, *i.e.*, molecular dynamics, large-scale computation, and etc., during I have worked as a technical staff. Dr. Yoshitaka Tateyama and Dr. Keitaro Sodeyama supported me from various areas of my study. Dr. Hiori Kino, Dr. Yusuke Otani gave me helpful advice about my work. Special thanks also to Dr. Ayako Nakata, Dr. Jun Haruyama, Dr. Lucie

Szabova for the support on my study life.

I want to thank all members of the Morihashi laboratory, my friends, and my co-workers.

I would like to close this acknowledgment by thanking my family.